ENE 503 – Computational Fluid Dynamics

WEEK 9: ARTICLE ASSIGNMENT 1

ARTICLE ASSIGNMENT 1:

- **Computational modelling of polymer injection molding:**

➢ Summary

Please summarize the numerical study conducted in the article

➢ Numerical modelling and simulation

In this section briefly discuss the following points

- How is the flow geometry created?
- Specify the boundary conditions defined on the surfaces.
- Compare compatibilities for computational modeling and simulation.
- What kind of computational nodes are used in the study?
- Is the mesh independence test performed? If it is so, analyze the results comparatively.
- Is there a validation study for computational modeling and simulation?
- Is a parametric study performed? If so, what are the results?

➢ Results of the article study

- Summarize the results of the study. Are there qualitative and quantitative results both presented in this study? What do these results indicate? What are the challenges of modelling of polymer injection process?

Proceedings of 6th ICCHMT
May 18–21, 2009, Guangzhou, CHINA
173

3-D NUMERICAL SIMULATION OF POLYMER INJECTION MOLDING

M. Tutar*& A. Karakus
Mersin University, Department of Mechanical Engineering, Ciftlikkoy, 33343, Mersin, Turkey
*Correspondence author: Fax: +90 324 3610258 Email: m_tutar@mersin.edu.tr

ABSTRACT
The numerical study of high-viscous non-isothermal fluid flow is performed considering the effects of phase changes and of the compressibility to simulate three-dimensional (3-D) filling process of mold-insert polymer injection molding. The volume of fluid (VOF) element method coupled with an implicit finite volume approach is utilized for the numerical computations. The user-defined functions are written to account for the changes in viscosity and density in the mold flow and are successfully incorporated into the VOF method coupled with a finite volume approach to generate more realistic melt flow physics during filling process of injection molding under different process conditions. The present numerical results are verified for a polypropylene (PP) pipe fitting model in comparison with the well-known commercial software Moldflow to determine the relative performance and modeling constraints of the present computations for the optimization of a design of polymer pipe fittings in a 3-D injection molding.

NOMENCLATURE
E	energy (kJ/kg)
g	gravity (N/kg)
h	enthalpy (kJ/kg)
k	thermal conductivity ($\mathrm{W/m^\circ C}$)
P	static pressure (Pa)
T	temperature ($^\circ$C)
T_w	wall temperature ($^\circ$C)
T_0	injection polymer melt temperature ($^\circ$C)
t	time (s)
U	inlet velocity (m/s)
v	velocity (m/s)
x	coordinate direction
y	coordinate direction
z	coordinate direction

Greek symbols
μ	molecular viscosity (Pa.s)
ρ	density ($\mathrm{kg/m^3}$)
τ	shear stress tensor ($\mathrm{N/m^2}$)

INTRODUCTION
Injection molding is an important manufacturing process for the production of large number of plastic parts with various dimensions by injecting a molten polymer into mold cavities. It usually consists of four successive stages as melting of the polymer, pumping the polymer to the mold cavity (injection), forming the polymer into the desired shape and cooling, and solidification. The success of the injection molding process highly depends upon performing these stages as a continuous process. The optimization of these existing stages and the development of new processing technologies have been continued with the aid of numerical and experimental studies. A great number of experimental and numerical studies have been conducted to investigate the injection molding process for optimization of existing processes and are well documented in the literature [1-6]. The Generalized Hele-Shaw (GHS) flow model introduced by Hieber and Shen [4] provided numerical computations with simplified solutions for non-isothermal, non-Newtonian flows in mold cavities and have been successful in predicting polymer melt flow in thin mold cavities. Since the 2-D Hele-Shaw flow model could not reproduce successful predictions for the simulation of polymer melt flow in thick mold cavities due to in accurate resolution of fountain effects, the later numerical studies have continues with three-dimensional (3-D) numerical studies [5,7]. The numerical study of Chang et al. [6] demonstrated that the simplified solutions of Hele-Shaw flow models could not give

accurate simulation solutions for the large gap-wise dimensions and the application of 3-D numerical models would be required for the accurate representation of basic flow features of polymer melt flow in the thick cavities.

Governing equations: The 3-D, compressible, and non-isothermal fluid flows are mathematically described by the conservation laws that are conservation of mass, conservation of momentum and conservation of energy. Continuity equation in conservation form of mass can be written as follows

$$\frac{\partial \rho}{\partial t} + \nabla \cdot (\rho \cdot \vec{v}) = 0 \qquad (1)$$

Conservation of momentum equation for an inertial reference frame in conservation form is described by:

$$\frac{\partial (\rho \vec{v})}{\partial t} + \nabla \cdot (\rho \vec{v}\vec{v}) = -\nabla p + \nabla \cdot (\bar{\tau}) + \rho \vec{g} \qquad (2)$$

The stress tensor $\bar{\tau}$ is given by:

$$\bar{\tau} = \mu[(\nabla \bar{v} + \nabla \bar{v}^{T}) - \frac{2}{3} \cdot \bar{v} I] \qquad (3)$$

Where I is unit tensor and second term on right hand side is effect of volume dilation. Energy equation in conservation form can be written as below

$$\frac{\partial (\rho E)}{\partial t} + \nabla \cdot (\vec{v}(\rho E + p)) = \nabla \cdot (k \nabla T) \qquad (4)$$

Where

$$E = h - \frac{p}{\rho} + \frac{v^2}{2} \qquad (5)$$

In solid regions, energy transport equation takes the following general form:

$$\frac{\partial}{\partial t}(\rho h) + \nabla (\vec{v} \rho h) = \nabla \cdot (k \nabla T) + S_h \qquad (6)$$

The second term on left-hand side of Equation 6 represents convective heat transfer due to rotational or translational motion of solids where the velocity field is computed from the motion specified for the solid zone. The terms on right-hand side of Eq. 6 are the heat flux due to conduction and volumetric heat sources within the solids respectively.

The Volume of Fluid (VOF) element: In the present study the VOF model, proposed by Hirt and Nichols [8] is used for polymer melt flow-air interface tracking, in which a surface tracking technique applied to a fixed Eulerian mesh. In this model, a single set of momentum equations is shared by the fluids and the volume fractions of each of the fluids in each computational cell are tracked through domain. The fields for all variables and properties are shared by phases and represents volume-averaged values as long as the volume fraction of each of the phases is known at each location. Thus the variables and properties in any given cell are either purely representative of one of the phases or representative of mixture of phases depending on the volume fraction values. Please refer to Ubbink and Issaa [9] for the details.

The viscosity and specific volume methods: A viscosity model which is based on Cross type equations [10] is adopted into the present finite volume fluid flow solver [11]. These equations are written by user-defined functions (macros written in C++ programming languages) to relate the viscosity changes to large strain rate, temperature and pressure variations in polymer flow and are successfully incorporated into the present VOF method. A specific volume model which is based on Tait equations [12] is used in the present simulations to enhance the modeling capabilities of the present VOF method. The user defined functions based on these equations are written in C++ programming languages to account for the density changes due to temperature and pressure variations in polymer melt flow and are successfully incorporated into the present VOF method. Variation of specific volume by pressure and temperature regarding $p-v-T$ modeling, classical empirical equation of state proposed by Tait [12] is also used. With use of the suggested specific volume model, the present VOF method is further improved to account for density changes as a function of temperature and pressure together compared to a simple model of the present fluid flow solver which accounts for the density changes only as a function of temperature.

Computational details:

The numerical solver: The Pressure-Implicit with Splitting of Operators (PISO) pressure velocity

coupling scheme based on the high degree of approximate relation between pressure and velocity is used for the present numerical solver [11]. PISO scheme takes more CPU time per iteration than SIMPLE algorithm but decreases the number iteration per convergence by applying additional corrections procedures. In PISO, three linearized momentum equations are solved for a guessed pressure values and with sequential pressure correction equation. The mass flux and pressure are then corrected. This process is repeated until predetermined tolerance limit achieved. Energy and flow equations are coupled to determine the heat transfer between polymer-air fluid side and mold wall. In solid region, conduction is also solved to show the temperature distribution in the mold. Three order of magnitude for volume fraction and flow field and six order of magnitude for energy equation of residual level drop is selected to convergence in this study. Energy, flow and volume fraction equations are solved explicitly. The courant number, c greater than one increases the numerical diffusion on transported volume fraction function so courant number, c=0.5 is selected for all computations in the presented study.

Geometry set-up and computational mesh: The 3-D geometry set up used for the present transient laminar simulations is seen in Fig. 1. A box shaped insert metal is located in the mold cavity. A runner and gate are also shown. The high resolution of mesh configurations consisting of triangular unstructured mesh cells are used for surfaces of mold cavity. 3-D tetrahedral cells starting from triangular boundary faces are then created to build up a 3-D computational domain. Because the skewness of the cells has a primary importance of the accuracy and the convergence characteristics of numerical procedures, computational domain is converted to a mesh system composed of polyhedral cells and is reordered using the Cutchill-McKee method. 2-D views of the computational domain of the mold cavity are illustrated in Fig. 2.

Boundary conditions: No slip boundary conditions ($u = v = w = 0$) are imposed at walls of mold cavity. The uniform injection rate condition for polymer melt is imposed at the inlet of the runner during the filling stage ($u = U$ *specified*, $v = w = 0$ and $f_1 = 1$, $f_2 = 0$ where f_1 and f_2 denote volume fractions of melt and air, respectively). Pressure outlet boundary condition is applied at air vents with $f_1 = 1$, $f_2 = 0$. Gauge pressure is set to zero to represent atmospheric boundary conditions.

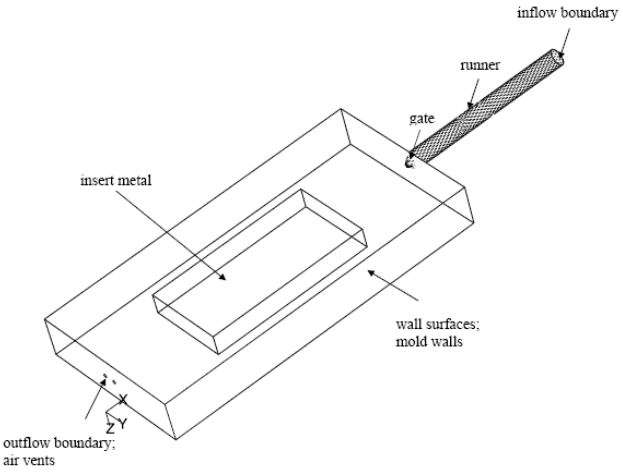

Figure 1
3-D geometry set-up

The impermeability condition is imposed at locations where the polymer melt make contact with the wall surfaces. The present simulations are carried out for two different injection rates and runner-to-gate diameter ratios, while mold wall temperature and injection polymer melt temperature are set to uniforms values of 313 K and 513 K, respectively. All process conditions and mesh resolutions used are presented in Table 1.

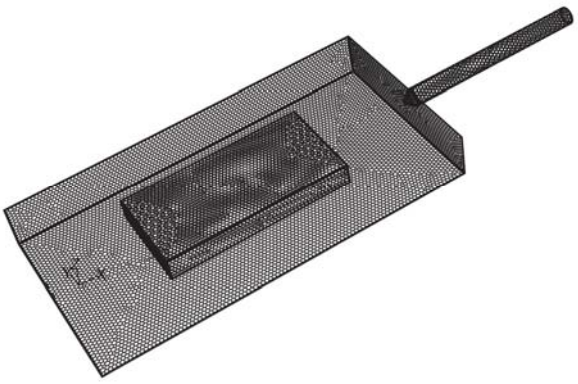

Figure 2
3-D computational mesh used in the present 3-d model simulations

Numerical model validation: To validate the present 3-D numerical model, a numerical test case is performed with constant material properties of the polymer melt and the air [5] in a two-dimensional (2-D) computational domain confined to a rectangular region between two parallel plates as seen in Fig. 3 (a). The present numerical model is validated against the experimental data of Behrens

[13] for the predicted positions of the polymer melt-air interface. The following parameters are defined according to the experimental data of Behrens [13]: x_{FT} is the flow tip of the current melt front, x_{CL} is the position of the contact line and *h* denotes the gap-wise thickness between the parallel plates. The comparison between the present model and the experimental data demonstrate that the present 3-D model predicts the positions of polymer melt flow front in a good agreement with the experimental data as seen in Fig. 3 (b) and can be used with a confidence for study of the effects of process conditions on the polymer melt flow in the further/subsequent section.

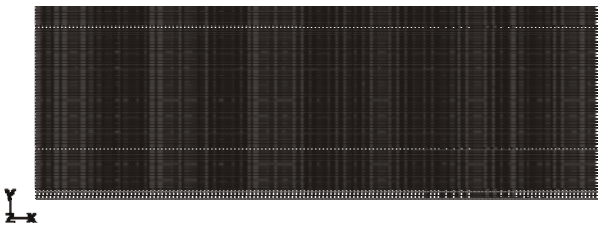

(a)

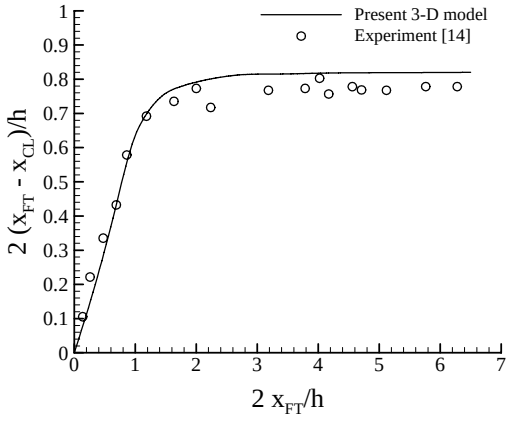

(b)

Figure 3
(a) Two-dimensional rectangular computational domain for the initial test validation;
(b) Comparisons of predicted polymer melt flow front positions

RESULTS AND DISCUSSION

3-D modeling of metal insert compressible injection molding process is performed using a numerical model developed in a finite volume based fluid flow solver [11]. User-defined functions are written in C++ programming language and are successfully incorporated into the present standard VOF formulation to account for the changes in viscosity, density and air-melt flow interface, and hence to accurately simulate the real molding conditions. The capabilities of the proposed numerical model in simulating mold insert injection molding processes are then assessed in comparison with the the well-known commercial package Moldflow MPI 3-D (the three dimensional model) [14] to optimize the polymer melt flow for different geometric and process conditions. Transient laminar simulations are performed until the bounded cavity is completely filled with the polymer melt flow. Filling stage of mold insert injection molding is simulated with different mesh resolutions, geometric dimensions (runner-to-gate diameter ratios) and polymer injection rates as summarized in Table 1. Two different gate diameters and injection rates are used for a pre-selected runner diameter of 2 mm to study effects of geometric dimensions and injection rate on the polymer melt flow. Three different mesh resolutions of polyhedral mesh elements are also studied for a chosen runner-to-gate diameter ratio of 2 to examine the effects of mesh resolutions on the simulation results.

Table 1
Process conditions and polyhedral meshes used

Cases	D_r/D_g	Injection rate (kg/s)	Temperature (K) Injection	mold	Mesh x 10^5
1	4	0.0015	513	313	0.9
2	2	0.0015	513	313	0.9
3	2	0.0015	513	313	1.35
4	2	0.0015	513	313	1.95
5	2	0.0010	513	313	1.95

To effectively describe the phase change effects, a solidification model based on enthalpy porosity technique is also used in all simulations. Present results are compared with each other and with those obtained from the Moldflow MPI 3-D model simulations on both qualitative and quantitative basis. The same geometry set up for each runner-to-gate diameter ratio and the corresponding similar mesh configurations and boundary conditions are also utilized for the Moldflow MPI 3-D model simulations to make a direct comparison with the solutions of the present numerical fluid flow solver. Upon completion of qualitative comparisons based on basic flow features, detailed quantitative comparisons are also made to further investigate the effects of geometric dimension and mass inflow rate on the present flow. The accuracy of the present

numerical methodology in predicting basic flow features such as flow symmetry, fountain flow and 3-D effects is initially verified against the well-know commercial software program Moldflow MPI as seen in Figs. 4 (a) and (b). The instantaneous 3-D polymer melt flow front appearance of Case 1 in Fig. 4 (a) indicates that the present 3-D model can successfully reproduce a round shape polymer melt flow front due to the fountain effects which are completely ignored by Hele-Shaw model applications. The predicted shape of the 3-D melt front topology and the flow symmetry with respect to the cavity centerline (Fig. 4 (b)) appears to be in a very good agreement with that of the Moldflow 3-D model as seen in Fig. 4 (b).

The fountain flow effects are also clearly discernable in a 2-D planer view in the transverse direction as seen in Fig. 5. “Fountain flow” is a flow phenomenon which is located near the polymer melt flow front and characterizes microstructure of molded plastic parts. It is also very important to accurately simulate the pressure and velocity variations at the melt flow front in the gap-wise direction. Figure 5 shows the capability of the proposed numerical methodology for predicting air traps and weld lines at the end of the filling simulation for Case 2. The instantaneous volume fraction contours on the mid-span symmetry plane at a simulation time of 1.2 s clearly present the predicted air traps (air concentration which can not be removed from the mold walls) around the corners of the mold cavity and weld lines due to remerging melt flow behind the insert. The flow symmetry is also predicted well with the present 3-D model. The polymer flow front advancements for Case 3 for the present 3-D model at distinct time instants is clearly illustrated in Fig. 6. The polymer melt flow advances in the mold cavity in a symmetrical manner with respect to the cavity centre line and is successfully represented by a 3-D curved shape at every time instant. In addition, the splitting and remerging of the flow front around the metal insert is successfully represented by the present model approach. Remerging behind the rear face of the insert, causes the weld line formation and the melt flow further advances to completely fill the mold cavity.

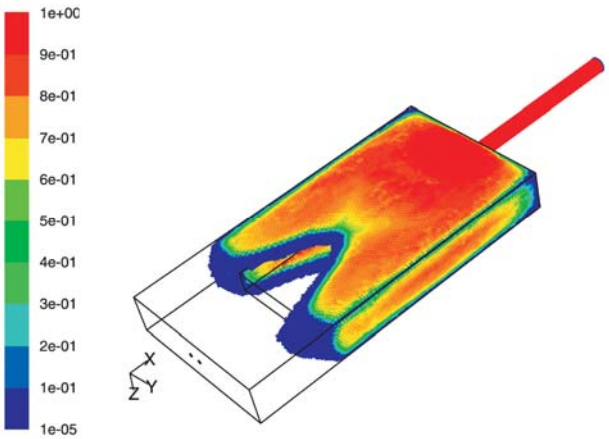

(a)

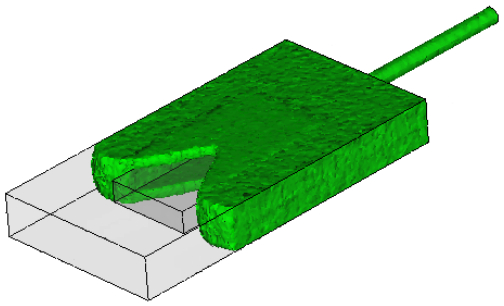

(b)

Figure 4
The instantaneous volume fraction contours for Case 1 at a simulation time of 1.1 s; (a) The present 3-D model; (b) Moldflow 3-D model

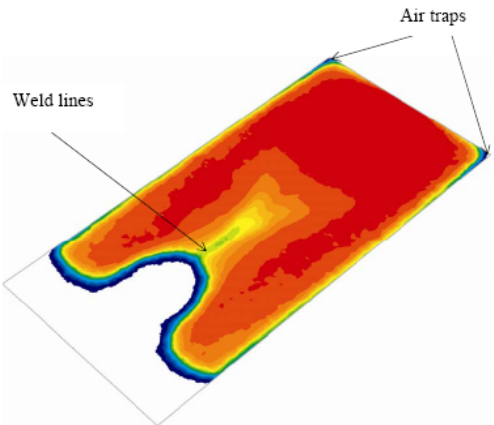

Figure 5
The instantaneous volume fraction contours on the mid-span symmetry plane at a simulation time of 1.2 s for Case 2

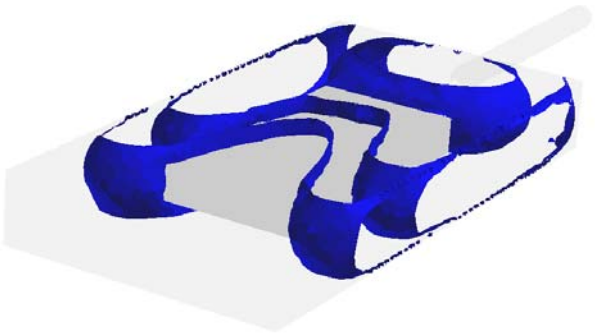

Figure 6
The evolution of polymer melt flow front for Case 3 for the present 3-D model at different time instants (t = 0.15 s, 0.7 s, 1.1 s)

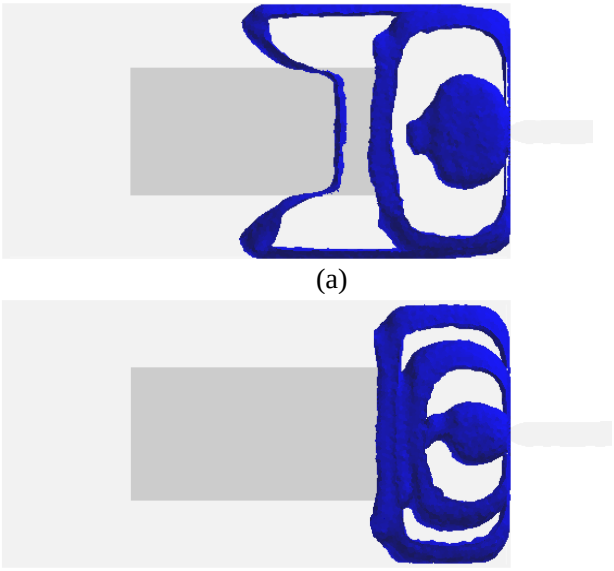

(a)

(b)

Figure 7
Polymer flow front evolutions with time at two different injection rates; (a) Case 4, $m^{\circ} = 0.0015$ kg/s; (b) Case 5, $m^{\circ} = 0.0010$ kg/s

Figures 7 (a) – (b) comparatively represent the 2-D views of instantaneous positions of the polymer melt flow fronts at two different injection rates. As seen in these figures, higher injection rate constitutes a better mechanism for an earlier confrontation of the polymer melt flow with the insert metal, resulting in further forward movement of melt flow in the mold cavity. This is probably due to higher momentum flow rate of polymer melt with increasing injection rate just before the gate exit. Higher injection rate also promotes viscous actions between adjacent polymer layers, which in turn, leads to increase of viscous heating and slightly higher temperature field distributions through the filled portion of the mold cavity as seen in Figs. 8 (a) and (b). Due to temperature difference between the insert walls and the injection polymer melt flow, significant temperature variations take place near the insert walls due to very high shear rates there.

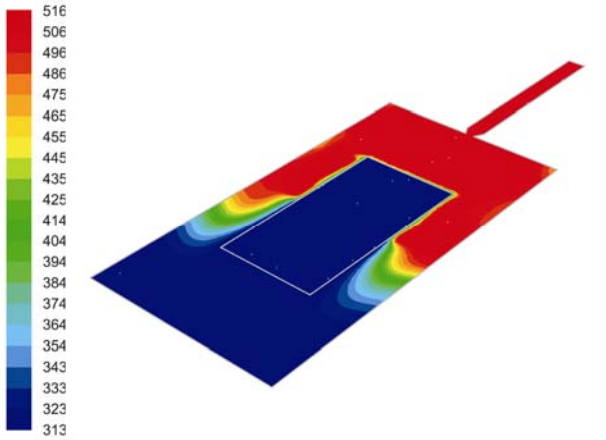

(a)

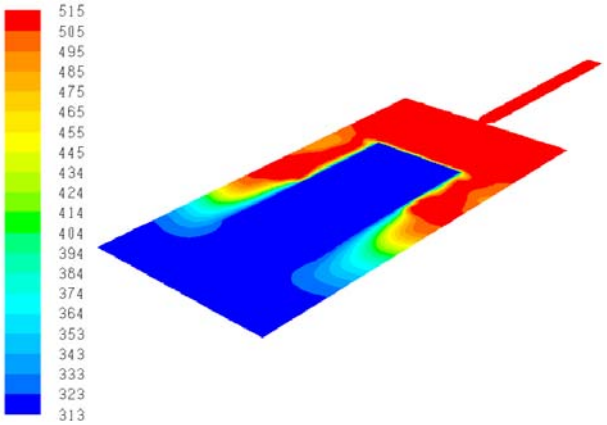

(b)

Figure 8
Instantaneous temperature distributions at two different injection rates at a simulation time of t = 0.41 s; (a) Case 4, $m^{\circ} = 0.0015$ kg/s; (b) Case 5, $m^{\circ} = 0.0010$ kg/s

Figures 9 (a) and (b) illustrate the evolutions of area -weighted average gate pressure for each case during the filling stage of the mold cavity. It is clearly seen in Fig. 9 (a) that a linear increase in pressure values during the very early stage of the filling process is observed due to flow resistance as previously noted by Bunchman et al. [15].

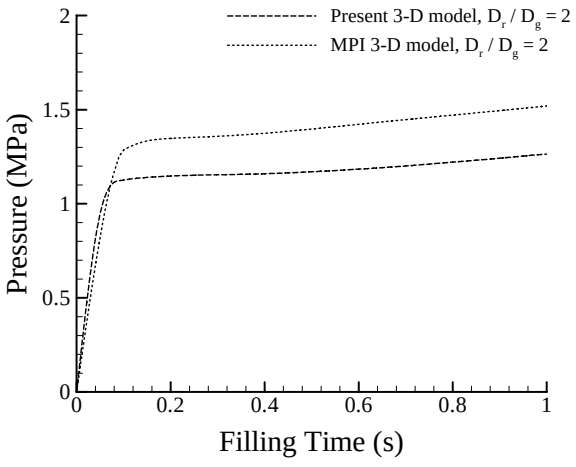

(a)

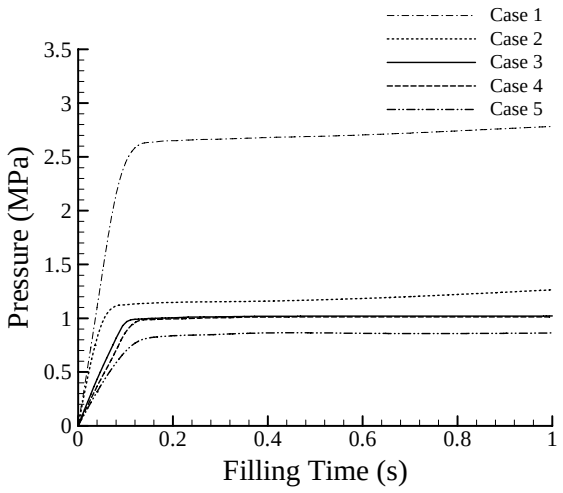

(b)

Figure 9
The calculated area-weighted average gate pressure evolutions for each case for the present 3-D model simulations

The present 3-D model simulations demonstrate a good indication of the predicted gate pressure evolutions. The results also correspond well with that of Moldflow MPI 3-D model except lower pressure values obtained from the present 3-D model. This is probably due to numerical differences for coupling velocity and pressure field parameters for these two model approaches. It is demonstrated in Fig. 9 (b) that the area- weighted average gate pressure evolution is significantly influenced by variations in geometric dimension. As the runner-to-gate diameter ratio is decreased from 4 to 2, the average pressure values obtained from each case considerably decreases. The injection rate also significantly influences the predicted gate pressure evolution and lower pressure values are obtained as the injection rate decreases. The momentum diffusion is much more pronounced with the increasing injection rate, which in turn, contributes the high shear rate in the polymer melt flow. Figure 9 (b) also indicates the influence of mesh resolution on the predicted gate pressure evolutions. The increase in mesh resolution after 135,000 polyhedral mesh cells does not influence much the predicted pressure evolution as observed in Fig. 9 (b).

CONCLUSIONS

Several conclusions can be drawn from the present study as below

1. The capabilities of the present numerical methodology in simulating compressible injection molding are considerably increased with the inclusion of user-defined functions into the VOF method. These functions account for the effects of viscosity changes and density variations to accurately simulate the real molding process.

2. The proposed numerical approach successfully reproduces the basic flow features such as the 3-D effects, flow symmetry, fountain flow, and gate pressure evolution. The results correspond well with those obtained from the Moldflow MPI 3-D model and the experimental data.

3. The model geometry used in the present study represents a realistic mold insert injection molding process with the construction of air vents through which air is pushed out of the mold cavity during the filling.

4. The effects of geometric dimensions on the present polymer melt flow seem to be more significant than the effects of injection rate. The geometric dimensions and configurations need to be considered carefully to optimize the injection molding process

5. The present results suggest that the developed numerical model can be used with a confidence for further numerical studies of injection molding processes provided that all process conditions are studied to optimize the flow.

ACKNOWLEDGMENTS

The authors of the present study would like to thank scientific and technical research council of turkey (Tubitak) for their financial support under the project no 106m465

REFERENCES

1. Gao, D.M., Nguyen, K.T., Hetu, J.F., Laroche, D., and Rejon A.G., 1998, Modeling of Industrial Polymer Process: Injection Molding and Blow Molding, Advanced Performance Material, **5**, pp. 43-64
2. Wang, T.H., Young W.B., 2005, Study on Residual Stress of Thin-Walled Injection Molding, European Polymer Journal, **41**, pp. 2511-2517
3. Courbebaisse, G., Garcia, D., 2002, Shape Analysis and Injection Molding Optimization, Computational Material Science, **25**, pp. 547-553
4. Hieber, C.A., Shen, S.F., 1980, A Finite-Element-Finite-Difference Simulation of the Injection-Molding Filling, J. of Non-Newtonian Fluid Mechanics, **7(1)**, pp. 1-32
5. Chang, R. Y., Yang, W. H., 2001, Numerical Modeling of Mold Filling in Injection Molding Using a Three-dimensional Finite Volume Approach, Int. J. of Numerical Methods, **37**, pp. 125-148
6. Chang, R.Y.,Yang, W.H., Hwang, S.J., Su, F., 2004, Three-Dimensional Modeling of Mold Filling in Microelectronic Encapsulation Process, IEEE Transactions on Components and Packaging Technologies, **27(1)**, pp. 200-209
7. Hetu, J.F., Gao, D.M., Garcia-Rejon, A., Salloum, G., 3D finite element method for the simulation of the filling stage in injection molding, Polymer Engineering Science, **38**, pp. 223-236.
8. Hirt C. W., and Nichols, B.D., 1981, A Computational Method for Pressure-Surface Hydrodynamics, J. of Pressure Vessel Technology, Transactions of the ASME, **103(2),** pp. 136-141
9. Ubbbink, O., Issaa, R. I., 1999, A Method for Capturing Sharp Fluid Interfaces on Arbitrary Meshes, J. Comp. Physics, **153**, pp. 26-50
10. Cross, M.M, 1979, Relation between viscoelasticity and shear-thinning behaviour in liquids, Rheologica ACTA, 18 pp. 609-614
11. Fluent Solver Version 6.3.26, 2006, Fluent Inc., Hamshire, USA
12. Tait, P. G., 1988, Physics and Chemistry of the Voyage H.M.S Challenger, **2(4)**, Scientific papers LXI
13. Behrens, R.A., Transient domain free surface flows and their application to mold filling; Ph. D. Thesis, University of Delaware 1983.
14. Moldflow, Moldflow Plastic Insight 3-D, Version 6.2, Moldflow Corporation, Wayland, MA, USA 2008
15. Bunchmann, M., Theriault, R., Osswald, T. A., 1997, Polymer Flow Length Simulation During Injection Mold Filling, **37 (3)**, pp. 667-671